J. Fluid Mech. (2013), *vol.* 737, R2, doi:10.1017/jfm.2013.582

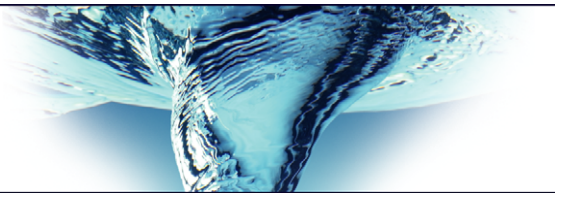

JFM RAPIDS
journals.cambridge.org/rapids

A swirling spiral wave solution in pipe flow

K. Deguchi† and A. G. Walton†

Department of Mathematics, Imperial College London, South Kensington Campus, London SW7 2AZ, UK

(Received 23 September 2013; revised 22 October 2013; accepted 24 October 2013; first published online 20 November 2013)

A numerically exact full Navier–Stokes counterpart of the asymptotic nonlinear solution in Hagen–Poiseuille flow proposed by Smith & Bodonyi (*Proc. R. Soc.* A, vol. 384, 1982, pp. 463–489) is discovered. The solution takes the form of a spiral travelling wave, with a novel feature being a strong induced component of swirl. Our solution shows excellent quantitative agreement with the asymptotic theory at Reynolds numbers of the order of 10^8.

Key words: critical layers, nonlinear instability, transition to turbulence

1. Introduction

Although more than 130 years have elapsed since the pioneering experiments of Osborne Reynolds (1883), our understanding of the pipe flow transition process is still far from complete. As a consequence, the study of the stability of flow through a pipe of constant circular cross-section subject to a uniform axial pressure gradient remains one of the most enduring and frequently studied problems in fluid mechanics. For many years the simple exact uni-directional solution (Hagen–Poiseuille flow, HPF) was the only one known to exist. This profile is linearly stable according to the weight of numerical evidence (e.g. Meseguer & Trefethen 2003) and therefore cannot be used as a springboard to identifying potential alternative nonlinear travelling-wave (TW) solutions of the governing Navier–Stokes equations. This difficulty was finally overcome in a numerical sense independently by Faisst & Eckhardt (2003) and Wedin & Kerswell (2004), who used artificial forcing to generate such solutions and were successful in continuing them to the unforced state. Since this major breakthrough, many other TW states have been identified (e.g. Pringle & Kerswell 2007; Duguet, Willis & Kerswell 2008), with some existing down to Reynolds numbers R as low as $R = O(10^3)$. These coherent states possess a three-dimensional roll–streak structure and are believed to scale according to vortex–Rayleigh wave interaction theory (Hall & Smith 1991; Hall & Sherwin 2010) in the limit of large Reynolds number.

† Email addresses for correspondence: k.deguchi@imperial.ac.uk, a.walton@imperial.ac.uk

Despite the success in generating these TW states, a puzzle remains. Prior to their discovery, a high-Reynolds-number asymptotic study by Smith & Bodonyi (1982*a*, henceforth referred to as SB) suggested that nonlinear helical travelling waves, not reliant on a roll–streak structure, could propagate in HPF. The fundamental disturbance is similar in nature to a large-amplitude Tollmien–Schlichting wave with a nonlinear, viscous critical layer. By asymptotic matching of the flow solution there to that in the surrounding inviscid region and the viscous wall layer, SB were able to determine explicitly the amplitude dependence of the neutral waves; this turned out to be of a relatively small size $O(R^{-1/3})$ in the majority of the flow field, but as large as the parabolic basic flow within the critical layer where the wave speed coincides with that of the basic flow. This structure is the only rational and analytic alternative solution to HPF known to date. Early attempts to discover this solution numerically were unsuccessful (Toplosky & Akylas 1988; Landman 1990) and it has been downgraded by some authors in more recent times to a 'suggestive analysis', rather than an actual solution.

The relevance of the SB analysis was cast into further doubt once other TW states were discovered numerically, for it was clear that, although helical roll–streak TW states have been found numerically (Pringle & Kerswell 2007), the SB solution has a rather different structure, being dependent purely on spiral wave and radial coordinates, and is essentially two-dimensional in nature. The SB solution is also characterized by a radially dependent azimuthal mean-flow distortion ('swirl'), and its presence is a necessary part of the flow structure, whereas it seems that in Pringle & Kerswell's solution any observed swirl is not an essential part of the self-sustaining mechanism. The impact of artificially introduced swirl disturbances to HPF have been investigated intensively in view of their ability to enhance heat exchange and mixing in engineering situations, although such an imposed swirl is found ultimately to decay (see Rocklage-Marliani, Schmidts & Ram 2003; Pashtrapanska *et al.* 2006; and references therein). Recently Deguchi & Walton (2013) have demonstrated numerically the connection between the essentially two-dimensional Tollmien–Schlichting wave-type asymptotic theories and full Navier–Stokes solutions, and this has increased the likelihood of finding a finite-Reynolds-number version of the SB TW structure in HPF, in which the swirl is an induced permanent feature of the flow.

In this paper we report our success in finding numerically such a swirling, helical solution for pipe flow at large but finite Reynolds number. Moreover, we show that in the limit of large Reynolds number this numerical solution agrees quantitatively with the structure proposed by SB. The method by which we find the spiral wave solution is based on the ideas of Walton (2002, henceforth referred to as W2002), who demonstrated asymptotically that the SB state could be reached from the linear stability of impulsively started pipe flow. The continuation procedure we use is outlined in § 2 together with its physical motivation, followed in § 3 by some brief details of the SB solution which are necessary for the comparisons we make with our numerical solution. The numerical method and results are discussed in §§ 4 and 5. The work on investigating the parameter space for this solution is still very much in its infancy, and some of the ideas concerning possible extensions are mentioned in the final section.

2. Formulation

We consider the unsteady, forced, incompressible Navier–Stokes equations in the non-dimensional form

$$\nabla \cdot \boldsymbol{u} = 0, \quad \partial_t \boldsymbol{u} + (\boldsymbol{u} \cdot \nabla)\boldsymbol{u} = -\nabla p + R^{-1}(\nabla^2 \boldsymbol{u} + \boldsymbol{f}) \tag{2.1}$$

in cylindrical coordinates (x, r, θ) spanned by unit vectors $\boldsymbol{e}_x$, $\boldsymbol{e}_r$ and $\boldsymbol{e}_\theta$, together with no-slip conditions at the pipe wall $r = 1$ and periodic conditions in the axial direction. Here the parameters governing the system are the Reynolds number R based on the pipe radius and the maximum velocity of the undisturbed HPF, axial wavenumber α and azimuthal wavenumber N. The specific forcing we choose acts purely in the axial direction and takes the form

$$\boldsymbol{f} = \boldsymbol{e}_x \sum_{n=1}^{\infty} \lambda_n^2 C_n \mathrm{J}_0(\lambda_n r) \exp(-\lambda_n^2 \tau), \quad C_n = \frac{8}{\lambda_n^3 \mathrm{J}_0'(\lambda_n)}, \tag{2.2}$$

where the λ_n are the zeros of the Bessel function J_0 and τ is a parameter. Clearly, as $\tau \to \infty$, the equations become unforced. A bifurcation analysis of the linear neutral forced state demonstrates the existence of a nonlinear TW solution propagating with phase speed c and dependent only on r and the spiral wave coordinate

$$\xi \equiv \alpha(x - ct) + N\theta. \tag{2.3}$$

Our approach is to use a continuation procedure to calculate TW states at increasing values of the extra parameter τ, with the ultimate aim of computing a TW state for unforced pipe flow as $\tau \to \infty$.

By way of contrast with some other approaches that have successfully used artificial forcing in the Navier–Stokes equations as a means of generating unforced TW states (e.g. Waleffe 1998; Faisst & Eckhardt 2003; Wedin & Kerswell 2004; Pringle & Kerswell 2007), the particular form for $\boldsymbol{f}$ in (2.2) can be motivated physically. We shall now describe why we have confidence that this approach will ultimately lead us to a numerically generated finite-Reynolds-number version of the SB solution.

The basic solution of (2.1) that corresponds to the specific forcing (2.2) has the form

$$\boldsymbol{u} = U_0(r; \tau)\boldsymbol{e}_x, \quad p = -4x/R, \quad U_0(r; \tau) = 1 - r^2 + \sum_{n=1}^{\infty} C_n \mathrm{J}_0(\lambda_n r) \exp(-\lambda_n^2 \tau). \tag{2.4}$$

This solution (first derived by Szymanski (1932)) corresponds to the development of impulsively started pipe flow under the influence of a constant axial pressure gradient and shows how HPF is attained as $\tau \to \infty$. The basic flow in (2.4) satisfies the (unforced) equation

$$\partial_\tau U_0 = 4 + (\partial_{rr}^2 + r^{-1}\partial_r)U_0 \tag{2.5}$$

subject to regularity at $r = 0$, no slip on $r = 1$ and zero flow at $\tau = 0$, with τ playing the role of time. The high-Reynolds-number stability properties of this basic flow as τ varies have been studied in W2002 and we mention here some of the key findings.

First, when τ is sufficiently small, the basic flow acquires a near-wall boundary-layer form which takes into account the smoothing effects of viscosity on the incoming plug flow. The first effects of pipe curvature on the stability characteristics are not experienced until $\tau \sim O(R^{-2/7})$ and linear growth of disturbances continues to occur until $\tau \sim O(R^{-2/9})$. On this latter scale a linear cut-off can be calculated such that, if τ exceeds this value, the flow is linearly stable. For example, for

$(N, \alpha) = (1, 0.4)$, there is no linear instability for $\tau R^{2/9} \gtrsim 0.5523$. It is the finite-$R$ equivalent of this neutral point that we will use in § 4 as the starting point for our computation. Returning to the asymptotic properties, W2002 shows that weakly nonlinear disturbances survive beyond this neutral point, with only minor changes necessary to the linear stability structure. The fluctuation amplitude, based on the Fourier decomposition of the pressure perturbation as

$$A = 2\sqrt{\sum_{n=1}^{\infty} |\hat{p}_n|^2}\Bigg|_{r=1}, \quad p = -\frac{4x}{R} + \hat{p}_0(r) + \sum_{n=1}^{\infty} \hat{p}_n(r) \mathrm{e}^{\mathrm{i}n\xi} + \text{c.c.}, \tag{2.6}$$

increases with τ in order to maintain an equilibrated state with the critical layer moving away from the pipe wall. Note that here we define the 'fluctuation' part as the ξ-dependent part of the solution. Eventually, at $O(1)$ values of τ, the critical layer moves to an $O(1)$ distance from the wall, and a new strongly nonlinear structure emerges. In the limit $\tau \to \infty$ this structure evolves into the asymptotic solution proposed by SB, provided that the disturbance azimuthal wavenumber N is unity. (For other integral values of N, the theory predicts a nonlinear cut-off at an $O(1)$ value of τ).

Thus, according to the asymptotic analysis, provided R is sufficiently large, it should be possible to compute TW solutions to the forced problem (2.1)–(2.2) and obtain a finite-Reynolds-number version of the SB structure as $\tau \to \infty$. Moreover, the asymptotic theory predicts that the amplitude of the disturbance is a monotonically increasing function of τ, suggesting a geometrically simple bifurcation process from the linear state. Of course, the main issue here is the largeness of the Reynolds number required to achieve this and the implications for the resolution of the numerical solution. This will be discussed in §§ 4 and 5 following a brief examination of the SB structure.

3. The Smith–Bodonyi solution

In the early 1980s, drawing on previous work concerning nonlinear critical layers (Benney & Bergeron 1969) and their own experience with nonlinear TW structures in boundary-layer flows (Smith & Bodonyi 1982*b*), SB proposed a high-Reynolds-number structure for a nonlinear helical TW in pipe flow. They found that in the majority of the pipe the wave is monochromatic and inviscid at leading order, with the resulting singularity smoothed out in a viscous nonlinear critical layer. There is also a thin viscous wall layer and it is the dynamical interplay between these two layers that underpins the solution structure. Somewhat surprisingly, the details of the critical layer could be determined analytically, and apart from a few relatively minor computations it proved possible for SB to determine the amplitude dependence of the neutral modes explicitly. This appeared to represent a major breakthrough in one of the most fundamental and enduring problems in fluid mechanics, especially as at that point in time no TW states in pipe flow had been discovered at finite Reynolds number. However, as mentioned in the introduction, attempts to find the SB solution numerically proved unsuccessful, and in recent times this structure has fallen into relative obscurity despite its intriguing properties. As stated earlier, our aim here is to bring this solution back to deserved prominence by determining it numerically from the Navier–Stokes equations using the continuation procedure outlined in § 2. To aid with this we describe in this section some of the key properties of the SB solution. For

more details of the solution the reader is referred to SB and also to the corrections in Walton (2005).

One of the main features of the SB solution is the dominance of the mean-flow distortion, whose axial and azimuthal components are comparable in size. This is evident in the core-flow expansions

$$u = 1 - r^2 + R^{-1/6}\overline{u}_{1M}(r) + O(R^{-1/3}), \quad w = R^{-1/6}\overline{w}_{1M}(r) + O(R^{-1/3}). \tag{3.1}$$

Here $\overline{w}_{1M}(r)$ is the swirling component referred to earlier. The fluctuation at next order is inviscid and therefore requires a viscous layer of thickness $O(R^{-1/2})$ near the pipe wall. The pressure expansion is

$$p + 4x/R = R^{-1/3}\{A_0 P_2(r)\cos\xi + P_{2M}(r)\} + O(R^{-1/2}\ln R), \tag{3.2}$$

which includes the unknown amplitude A_0. The pressure function P_2 in (3.2) and leading-order phase speed c_0, where the phase speed expands as $c = c_0 + O(R^{-1/6})$, are found, for given wavenumbers α, N, from the solution of the Rayleigh eigenvalue problem

$$(1 - r^2 - c_0)(P_2'' + r^{-1}P_2' - (\alpha^2 + N^2/r^2)P_2) = -4rP_2' \tag{3.3}$$

subject to regularity on $r = 0$, the tangential flow constraint $P_2'(1) = 0$ and the condition of zero phase shift across the critical level $r = r_c$, where $c_0 = 1 - r_c^2$. A nonlinear critical layer of thickness $O(R^{-1/6})$ in the vicinity of $r = r_c$, where there is a complicated dependence on a combination of the radial and spiral wave coordinates, in contrast to the core fluctuation solution, is necessary to smooth out the inviscid singularities that arise in the velocity and pressure perturbations. SB discovered numerically that a suitable solution to (3.3) can only be found if $N = 1$. Once the phase speed and pressure are determined, the amplitude A_0 of the fluctuation follows from the explicit expression

$$A_0 = \frac{N^{4/3}c_0^{5/3}\alpha^{5/3}r_c^{2/3}}{2^{1/3}(N^2+\alpha^2)^{2/3}(N^2+\alpha^2 r_c^2)P_2(r_c)}\left(\frac{P_2(r_c)}{P_2(1)}\right)^{4/3}|12C^{(1)} + 4\pi + D^{(1)}|^{2/3}. \tag{3.4}$$

This formula, which emerges after a detailed analysis of the nonlinear critical layer, is as in SB's equation (3.26), but with the addition of the extra constant $D^{(1)}$, which was missed in their original analysis and subsequently introduced by Walton (2005). The two constants $C^{(1)}$ and $D^{(1)}$ need to be calculated numerically and take the approximate values

$$C^{(1)} \simeq -5.516, \quad D^{(1)} \simeq 20.858. \tag{3.5}$$

The leading-order radial velocity in the core is given in terms of the pressure as

$$v = R^{-1/3}V_2(r)\sin\xi + O(R^{-1/2}\ln R), \quad V_2(r) = -\frac{A_0 P_2(r_c)P_2'(r)}{\alpha(1 - r^2 - c_0)}. \tag{3.6}$$

The mean-flow distortions in (3.1) are not written down explicitly in SB but can be calculated fairly easily by proceeding to higher order. It turns out that they possess the simple forms

$$\overline{u}_{1M}(r) = \begin{cases} M_1 & (0 \leqslant r < r_c), \\ M_2 \ln r & (r_c < r \leqslant 1), \end{cases} \qquad \overline{w}_{1M}(r) = \begin{cases} M_3 r & (0 \leqslant r < r_c), \\ M_4(r - 1/r) & (r_c < r \leqslant 1). \end{cases} \tag{3.7}$$

The coefficients $M_i(\alpha)$ are fixed by the critical-layer analysis and can be expressed explicitly in terms of A_0 and r_c. In order to determine these coefficients numerically,

the Rayleigh equation (3.3) needs to be solved, and this is achieved using the same series solution method outlined in SB. This leads to the following values for some of the key quantities in the SB solution for the case $\alpha = 0.4$:

$$r_c \simeq 0.8133, \quad c_0 \simeq 0.3386, \quad P_2(1)/P_2(r_c) \simeq 0.9925, \quad A_0 P_2(r_c) \simeq 0.2092, \tag{3.8a}$$

$$M_1 \simeq -3.9035, \quad M_2 \simeq 1.0479, \quad M_3 \simeq 0.8043, \quad M_4 \simeq 1.3099. \tag{3.8b}$$

In § 5 we will make a quantitative comparison between the SB solution and our numerically generated TW for $\alpha = 0.4$ using the values given in (3.8).

4. Numerical method

We explicitly seek spiral wave-type solutions of (2.1) by decomposing the velocity field as

$$\boldsymbol{u} = (U_0 + \overline{u})\boldsymbol{e}_x + \overline{w}\boldsymbol{e}_\theta + \boldsymbol{\nabla} \times \boldsymbol{\nabla} \times (\phi \boldsymbol{e}_r) + \boldsymbol{\nabla} \times (\psi \boldsymbol{e}_r), \tag{4.1}$$

where U_0 is given in (2.4) and $\overline{u}$ and $\overline{w}$ are the mean-flow distortions. The poloidal and toroidal potentials for the fluctuation field are expanded by Fourier series as

$$\phi(r, \xi) = \sum_{n=1}^{M} \Phi_n(r) \mathrm{e}^{\mathrm{i}n\xi} + \text{c.c.}, \quad \psi(r, \xi) = \sum_{n=1}^{M} \Psi_n(r) \mathrm{e}^{\mathrm{i}n\xi} + \text{c.c.} \tag{4.2}$$

The phase speed c in the definition of spiral coordinate ξ in (2.3) is to be calculated as part of the solution for given values of R, τ, α and N.

The boundary conditions are regularity along $r = 0$ and no slip on the pipe surface $r = 1$. For $N = 1$, one possible choice of radial expansion that satisfies these conditions is

$$\Phi_n(r) = \begin{cases} r(1-r^2)^2 T^{even}(r) & \text{if } n = 0, \\ r^3(1-r^2)^2 T^{even}(r) & \text{if } n \neq 0 \text{ and } n \text{ is even}, \\ r(1-r^2)^2 T^{odd}(r) & \text{if } n \text{ is odd}, \end{cases} \tag{4.3}$$

$$\Psi_n(r) = \begin{cases} r(1-r^2) T^{even}(r) & \text{if } n \text{ is even}, \\ r(1-r^2) T^{odd}(r) & \text{if } n \text{ is odd}, \end{cases} \tag{4.4}$$

$$\overline{u}(r) = (1-r^2) T^{even}(r), \tag{4.5}$$

$$\overline{w}(r) = r(1-r^2) T^{even}(r). \tag{4.6}$$

If we expand $T^{even}(r)$ and $T^{odd}(r)$ in terms of some even and odd polynomials with minimum order n, the velocity components are analytic since in Cartesian coordinates the flow field is approximated by polynomials. When the centreline is not included in the computation, we need only consider the form of the Taylor expansion of the solution around $r = 0$. Here we approximate $T^{even}(r)$ and $T^{odd}(r)$ by sums of the first $L + 1$ even and odd Chebyshev polynomials, respectively. Substituting these expansions into (2.1) and discretizing the equations at the collocation points $r = r_k$, where

$$r_k = \cos\left(\frac{k+1}{2L+4}\pi\right), \quad k = 0, \ldots, L, \tag{4.7}$$

we obtain algebraic equations which can be solved by the Newton–Raphson iterative method. The algebraic equations include the condition

$$C_V(0.5) = 0 \tag{4.8}$$

to eliminate phase redundancy, where the $\cos\xi$ and $\sin\xi$ coefficients of the wall-normal velocity are defined as

$$C_V(r) \equiv \frac{1}{2\pi}\left(\int_0^{2\pi} v\mathrm{e}^{-\mathrm{i}\xi}\,\mathrm{d}\xi + \text{c.c.}\right), \quad S_V(r) \equiv \frac{\mathrm{i}}{2\pi}\left(\int_0^{2\pi} v\mathrm{e}^{-\mathrm{i}\xi}\,\mathrm{d}\xi - \text{c.c.}\right), \quad (4.9)$$

respectively. We terminate the iterations when the signal-to-noise-floor ratio reaches $O(10^{-10})$. More detail concerning the computational method can be found in Deguchi & Walton (2013).

According to the asymptotic analysis, the solution has a rapidly varying structure in the vicinity of the pipe wall. Thus we can expect better spectral convergence by mapping the radial coordinate $r \in [0, 1]$ to

$$\hat{r}(r, q) = \frac{\mathrm{e}^{q(r-1)} - \mathrm{e}^{-q}}{1 - \mathrm{e}^{-q}} \in [0, 1]. \quad (4.10)$$

The map parameter q specifies the extent to which grid points are clustered in the near-wall region, and if $q = 0$, then $\hat{r} = r$. This approach can be used in conjunction with the Chebyshev method with collocation points $\hat{r}_k = \hat{r}(r_k, q)$ with r_k given in (4.7) for the approximation of T^{even} and T^{odd}. We confirm that the result is insensitive to the choice of the map parameter q provided the solution is fully resolved, i.e. the upper limit M on the sums in (4.2) is taken sufficiently large. The mapping method described here proved vital for obtaining converged solutions at large amplitude. The parameter value $q = 4$ is used throughout the next section.

5. Numerical results

In what follows we concentrate on the case $\alpha = 0.4, N = 1$. In the future we plan to investigate parameter space more fully, but the computations are extremely expensive and so for present purposes it suffices to study the solution for a representative $O(1)$ value of α and concentrate on an azimuthal wavenumber of unity as this is the only value for which the SB solution appears to exist according to the asymptotic theory.

After several unsuccessful attempts at smaller Reynolds numbers (where we encountered a turning point at a finite value of τ), we were able to find a Reynolds number for which our solution extends all the way to $\tau = \infty$, where it represents an exact solution of the unforced Navier–Stokes equations. Figure 1 shows the result of a numerical computation at $R = 6 \times 10^8$. We start from the linear neutral point at $\tau = 0.0124$ and use our continuation strategy to compute solutions at increasing values of τ. As τ increases and the solution becomes more nonlinear, the number of Fourier modes and Chebyshev polynomials required for adequate resolution increases significantly. It is also necessary to take relatively small steps in τ in order that the Newton method converges satisfactorily. In figure 1(*a*) we plot the scaled amplitude $R^{1/3}A$ versus τ and observe that it approaches a constant value calculated as $\tau \to \infty$ (dot-dashed line), which is close to the corresponding asymptotic quantity in SB, $A_0 P_2(1)$ (dashed line). We can see from this result that the solution computed at $\tau = 2$ is extremely close to that found in the limit $\tau \to \infty$: in fact, at this value of τ the basic flow is within $O(10^{-5})$ of the parabolic profile at all values of r. The convergence towards the asymptotic solution can also be seen in figure 1(*b*), where the phase speed c also eventually shows good agreement with the SB theory, particularly bearing in mind that the corresponding SB quantity is only correct to $O(R^{-1/6})$. The largeness of the Reynolds number involved necessarily means that we require a considerable number of points near the pipe wall: certain resolution tests are

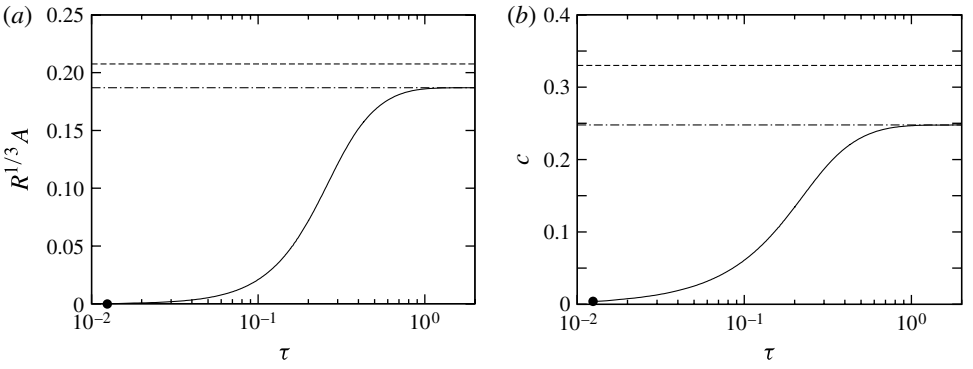

FIGURE 1. The bifurcation of the TW solution branch in forced pipe flow for $R = 6 \times 10^8$ and $\alpha = 0.4$: (*a*) scaled amplitude $R^{1/3}A$; and (*b*) phase speed c. The corresponding values in the limit of $\tau \to \infty$ and the SB theory for $\tau, R \to \infty, A_0 P_2(1)$ for (*a*) and c_0 for (*b*) are indicated by the dot-dashed and dashed lines, respectively. The truncation level $(L, M) = (360, 18)$ is used to draw the curves. The linear critical point is indicated by the filled circles.

(L, M)	A	c
(360, 28)	1.7896×10^{-4}	0.24498
(360, 30)	1.7884×10^{-4}	0.24456
(420, 30)	1.9700×10^{-4}	0.24625
(440, 30)	1.9715×10^{-4}	0.24643

TABLE 1. The convergence of the fully developed pipe flow solution for $(\alpha, N, R) = (0.4, 1, 10^9)$.

therefore necessary in order to confirm the validity of our numerical solutions. For the highest value of R in this paper, 10^9, we are satisfied that our solution for fully developed pipe flow is adequately resolved with 30 Fourier modes and 440 Chebyshev polynomials as shown in table 1: in what follows, we choose $(L, M) = (390, 30)$ for $R = 6 \times 10^8$ and $(L, M) = (420, 30)$ for $R = 8 \times 10^8$ by a similar resolution analysis.

An important feature of the SB solution is the $O(R^{-1/6})$ mean-flow distortion and in particular the presence of a swirl component $R^{-1/6}\overline{w}_{1M}(r)$ in (3.1), which is not evident in any previous nonlinear pipe flow TW computations. In figure 2 we plot the distortions as calculated from our computations and compare them with the asymptotic formulae (3.7). The agreement is remarkable, particularly bearing in mind that there are no free parameters to tune and that the next term in the asymptotic theory is $O(R^{-1/3})$: moreover the agreement improves as R is increased.

Next we provide the visualizations for the fluctuation part of the solution for $R = 6 \times 10^8$. At a fixed pipe cross-section the streamwise velocity and vorticity are pictured in figure 3(*a*,*b*), respectively. Note that these figures are sufficient to provide the entire visualization, since the solution depends only on r and ξ defined by (2.3) and the pattern at any other axial position is given simply by a rotation of the present figures. The critical layer structure is evident in these plots and is consistent with the SB theory, which predicts a rapid variation in the leading-order axial and azimuthal fluctuation velocities at the critical layer. Outside of the critical layer, the fundamental Fourier mode dominates the flow structure as the asymptotic theory predicts.

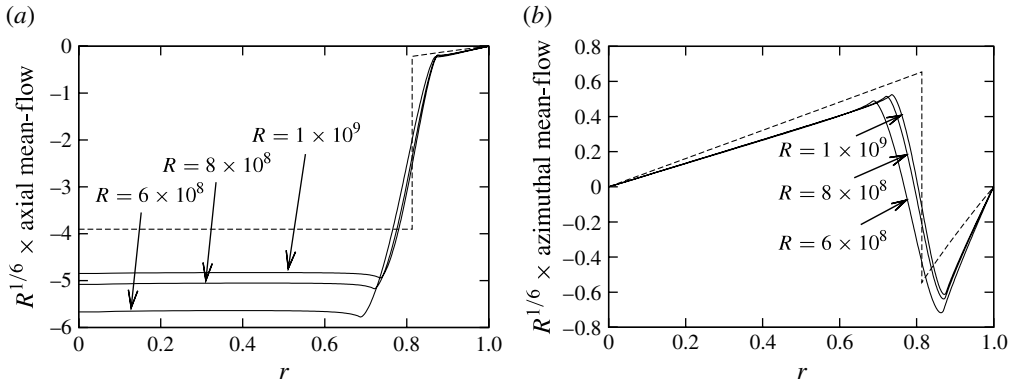

FIGURE 2. Comparison of the mean-flow distortions. The solid curves are the full Navier–Stokes computations, which apparently asymptote to the SB theory result (indicated by the dashed curves). (*a*) $R^{1/6}\overline{u}$ for the solid curves and $\overline{u}_{1M}$ for the dashed curve. (*b*) $R^{1/6}\overline{w}$ for the solid curves and $\overline{w}_{1M}$ for the dashed curve.

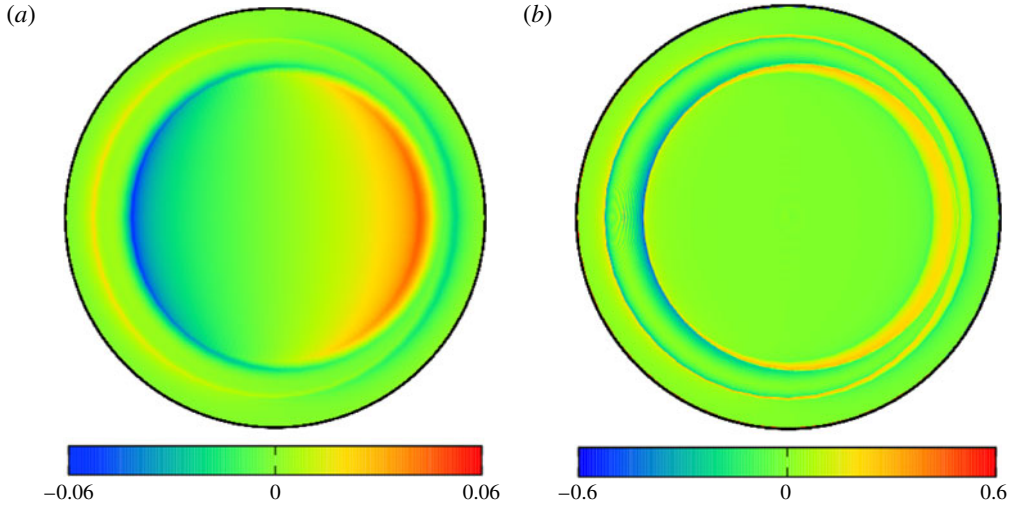

FIGURE 3. The fluctuation field for the fully developed TW solution at pipe cross-section $\xi = 0$ with $R = 6 \times 10^8$: (*a*) streamwise velocity, and (*b*) streamwise vorticity.

As a final comparison with the SB theory we plot the $\sin\xi$ component of the radial velocity in figure 4(*a*) and compare this with the SB expression in (3.6). Again we can see that the agreement improves with increasing Reynolds number. Consistent with the asymptotic theory, the $\cos\xi$ component of the radial velocity, shown in figure 4(*b*), is much smaller than the $\sin\xi$ component. In the inset in figure 4(*b*) we can see the existence of the thin viscous near-wall boundary layer, which is also an important feature of the SB solution. From these comparisons it seems clear that as $R \to \infty$ the TW solution for pipe flow that we have computed is indeed precisely the solution proposed by SB in their 1982 paper. This is the first time this structure has been detected numerically.

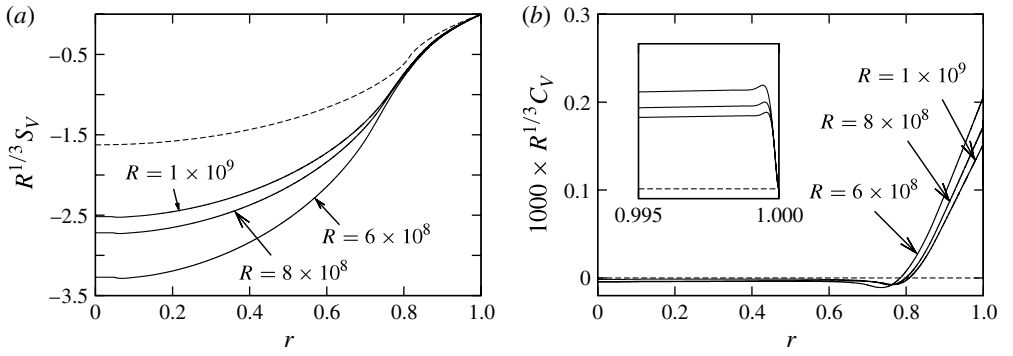

FIGURE 4. Comparison of the radial fluctuation velocities: (a) $\sin\xi$ component; (b) $\cos\xi$ component. The solid lines are the quantities in (4.9) calculated from the full Navier–Stokes results. The dashed lines are the leading-order asymptotic results: V_2 for (a) and zero for (b).

6. Discussion

In this study we have concentrated exclusively on the high-Reynolds-number properties of our swirl-dominated spiral TW solution with the aim of demonstrating a connection to the asymptotic structure of SB. Now that this has been established, it is worth remarking that the large value of R in this paper is not completely unrealizable in practice: for example, widely used Moody diagrams for engineering purposes usually cover $R = O(10^8)$; in addition, recent experimental turbulent pipe flow measurements have reached Reynolds numbers exceeding 10^6 and have detected a qualitative change of the near-wall scaling law (Hultmark *et al.* 2012). It is of course of interest to investigate the behaviour of the solution at lower Reynolds numbers by continuation in R from our present solutions in the future. It might be suspected that the internal and wall layers will thicken as R is decreased and although, on the face of it, radial resolution should be less of an issue, the disturbance is unlikely to remain dominated by one Fourier mode and therefore ensuring sufficient azimuthal resolution will be a challenging computational problem.

The dependence on axial wavenumber α is also of much interest. The SB solution breaks down in both the $\alpha \to 0$ and $\alpha \to \infty$ limits. In the former case, according to the asymptotics, the critical and wall layers thicken and merge with the core, all harmonics in the fluctuation assume equal importance and the governing equations become the so-called 'reduced' Navier–Stokes equations (e.g. W2002). These equations have been studied numerically recently in other geometries (Deguchi & Walton 2013; Deguchi, Hall & Walton 2013) and localized solutions, thought to be related to turbulent spots, have been discovered. It will be interesting to see if similar structures emerge in pipe flow, although such calculations will require a high degree of resolution in the spiral coordinate direction. In the $\alpha \to \infty$ limit a new asymptotic structure forms in which the critical layer moves to the pipe centre and disturbances propagate close to the maximum speed of the basic flow. This structure has been linked tentatively to the formation of slugs of vorticity (Smith, Doorly & Rothmayer 1990). Investigating such a structure numerically will be highly non-trivial and is likely to require the development of more sophisticated meshing techniques than those adopted here in view of the extreme separation of the critical and wall layers. The existence of the solution for other values of azimuthal wavenumber N

could, in principle, also be studied provided some care is taken over the choice of basis function. As mentioned before, however, the asymptotics predict (for $O(1)$ values of α) a solution of this form only when $N = 1$.

Finally, the connection between our solution and pipe entrance flow is evidently an area of considerable theoretical and practical interest. Although the Reynolds number used in this paper is large compared to the transition threshold originally observed in Reynolds (1883), it is likely that a similar nonlinear critical-layer structure emerges in such experiments and persists in the fully developed case, particularly when we recall that in a non-parallel flow such as that over a flat plate the Tollmien–Schlichting route to transition is often the preferred one. When the present structure comes into existence, it may play an important role in the basin of attraction of the laminar and turbulent states, since the SB disturbance energy, of $O(R^{-1/3})$, is considerably smaller than the $O(1)$ energy typically associated with roll–streak type solutions.

Acknowledgements

We thank the referees for their comments. A.G.W. would like to express his gratitude to Professor F. T. Smith F.R.S. for introducing him to this problem and for many insightful discussions over the years.

References

BENNEY, D. J. & BERGERON, R. F. 1969 A new class of nonlinear waves in parallel flows. *Stud. Appl. Maths* **48**, 181–204.

DEGUCHI, K., HALL, P. & WALTON, A. G. 2013 The emergence of localized vortex–wave interaction states in plane Couette flow. *J. Fluid Mech.* **721**, 58–85.

DEGUCHI, K. & WALTON, A. G. 2013 Axisymmetric travelling waves in annular sliding Couette flow at finite and asymptotically large Reynolds number. *J. Fluid Mech.* **720**, 582–617.

DUGUET, Y., WILLIS, A. P. & KERSWELL, R. R. 2008 Transition in pipe flow: the saddle structure on the boundary of turbulence. *J. Fluid Mech.* **613**, 255–274.

FAISST, H. & ECKHARDT, B. 2003 Traveling waves in pipe flow. *Phys. Rev. Lett.* **91**, 224502.

HALL, P. & SHERWIN, S. 2010 Streamwise vortices in shear flows: harbingers of transition and the skeleton of coherent structures. *J. Fluid Mech.* **661**, 178–205.

HALL, P. & SMITH, F. T. 1991 On strongly nonlinear vortex/wave interactions in boundary-layer transition. *J. Fluid Mech.* **227**, 641–666.

HULTMARK, M., VALLIKIVI, M., BAILEY, S. C. C. & SMITS, A. J. 2012 Turbulent pipe flow at extreme Reynolds numbers. *Phys. Rev. Lett.* **108**, 094501.

LANDMAN, M. J. 1990 On the generation of helical waves in circular pipe flow. *Phys. Fluids* **2**, 738–747.

MESEGUER, A. & TREFETHEN, L. N. 2003 Linearized pipe flow to Reynolds numbers 10^7. *J. Comput. Phys.* **186**, 178–197.

PASHTRAPANSKA, M., JOVANOVIC, J., LIENHART, H. & DURST, F. 2006 Turbulence measurements in a swirling pipe flow. *Exp. Fluids* **41**, 813–827.

PRINGLE, C. C. T. & KERSWELL, R. R. 2007 Asymmetric, helical and mirror-symmetric travelling waves in pipe flow. *Phys. Rev. Lett.* **99**, 074502.

REYNOLDS, O. 1883 An experimental investigation of the circumstances which determine whether the motion of water will be direct or sinuous, and of the law of resistance in parallel channels. *Phil. Trans. R. Soc. Lond.* A **174**, 935–982.

ROCKLAGE-MARLIANI, G., SCHMIDTS, M. & RAM, V. I. V. 2003 Three-dimensional laser-Doppler velocimeter measurements in swirling turbulent pipe flow. *Flow Turbul. Combust.* **70**, 43–67.

SMITH, F. T. & BODONYI, R. J. 1982*a* Amplitude-dependent neutral modes in the Hagen–Poiseuille flow through a circular pipe. *Proc. R. Soc. Lond.* A **384**, 463–489 (referred to herein as SB).

SMITH, F. T. & BODONYI, R. J. 1982*b* Nonlinear critical layers and their development in streaming-flow stability. *J. Fluid Mech.* **118**, 165–185.

SMITH, F. T., DOORLY, D. J. & ROTHMAYER, A. P. 1990 On displacement-thickness, wall-layer and mid-flow scales in turbulent boundary-layers and slugs of vorticity in channel and pipe flows. *Proc. R. Soc. Lond.* A **428**, 255–281.

SZYMANSKI, P. 1932 Quelques solutions exactes des équations de l'hydrodynamique du fluide visqueux dans le cas d'un tube cylindrique. *J. Math. Pures Appl.* **11**, 67–107.

TOPLOSKY, N. & AKYLAS, T. R. 1988 Nonlinear spiral waves in rotating pipe flow. *J. Fluid Mech.* **190**, 39–54.

WALEFFE, F. 1998 Three-dimensional coherent states in plane shear flows. *Phys. Rev. Lett.* **81** (19), 4140–4143.

WALTON, A. G. 2002 The temporal evolution of neutral modes in the impulsively started flow through a circular pipe and their connection to the nonlinear stability of Hagen–Poiseuille flow. *J. Fluid Mech.* **457**, 339–376 (referred to herein as W2002).

WALTON, A. G. 2005 The stability of nonlinear neutral modes in Hagen–Poiseuille flow. *Proc. R. Soc. Lond.* A **461**, 813–824.

WEDIN, H. & KERSWELL, R. R. 2004 Exact coherent structures in pipe flow: travelling wave solutions. *J. Fluid Mech.* **508**, 333–371.